Dear Editors,

We would like to submit the enclosed manuscript entitled “THIN SHEET AUTOMATIC INTERPRETATION OF DIKE SWARM MAGNETIC TRANSECTS USING REGULARIZED DERIVATIVES” as a non-peer reviewed preprint to EarthArXiv. This preprint was not under evaluation from a peer review journal. Automatic interpretation is an important topic in interpreting magnetic anomalies but, to our knowledge, few of the available techniques are effective when applied to multiple juxtaposed dikes as observed in dike swarms. We introduce a procedure that shows effectiveness in determining a minimum number of dikes compatible with the observed data as well as to automatic location of associated dike unities. Computer codes in MATLAB are provided to extend synthetic simulations and replication with a real data set. As a corresponding author, I declare no conflict of interest associated with this contribution as well as the co-authors agreement with the manuscript content.

Sincerely yours,

Carlos Mendonça
(carlos.mendonca@iag.usp.br)

THIN SHEET AUTOMATIC INTERPRETATION OF DIKE SWARM MAGNETIC TRANSECTS USING REGULARIZED SECOND DERIVATIVES

Carlos Alberto Mendonça,
University of São Paulo, Department of Geophysics, Rua do Matão, 1226, São Paulo, 05508-090, SP, Brazil. carlos.mendonca@iag.usp.br

Felipe Lisbona Cavalcante,
University of São Paulo, Department of Geophysics, Rua do Matão, 1226, São Paulo, 05508-090, SP, Brazil. felipe.cavalcante@usp.br

Janaína Anjos Melo
University of São Paulo, Department of Geophysics, Rua do Matão, 1226, São Paulo, 05508-090, SP, Brazil. janaina.melo@usp.br

COMPUTER CODE AVAILABILITY:

Program ATSInterp v.0 -Automatic Thin-Sheet Interpretation is made available at

https://github.com/camendonca697/ATSInterp_v0.git

ABSTRACT

Dike swarms are major continental structures recording large igneous provinces and crustal extension processes generating rifts and sedimentary basins. A key point in dike swarm studies is determining a minimum number of dikes that are necessary to explain the observed magnetic anomalies and inferences about position and depth for specific unities. We develop an automatic interpretation procedure to interpret the complex anomalies resulting from densely juxtaposed dikes forming a swarm, each dike with different depth and magnetization attributes. The automatic parameter estimation is based on the ratio of the amplitude of the magnetic anomaly (AMA) by its second-order derivative, the dike position and depth determined from simple algebraic expressions based on the thin-sheet model representation. The second derivative of the AMA serves to individualize intervals with specific dike units, thereby determining a minimum number of dikes based on their sharp or subtle concave-down expressions in the AMA profile. Tikhonov regularization is applied to prevent noise enhancing in evaluating numerical derivatives using a finite-difference scheme. A set of MATLAB programs are presented to evaluate the automatic interpretation of magnetic transects, a profile across the Ponta Grossa Dike Swarm in Southern Brazil serving as a testing data set since its results can be compared with a published dike model obtained from data inversion. Dike location and depth obtained with the automatic procedure accurately recover the model parameters obtained from nonlinear data inversion suggesting the utility of the proposed procedure to obtain a reliable model from complex anomalies.

INTRODUCTION

Large igneous provinces are associated to flood basalts, sills and plutonic layered systems usually connected by multi-stages dike intrusions plumbing magma across different crustal levels. The real extension and complexity of sheeted dike swarms were revealed as regional-long magnetic lineaments when aeromagnetic databases were compiled by companies and geological surveys. Aeromagnetic lineaments are useful in revealing the extension of subsurface tabular magnetic bodies but rarely the observed magnetic anomalies are one-by-one associated to single out cropping dikes. It is then assumed that most bodies may be seated at deeper levels, as such relying on magnetic data interpretation to infer dike location and related magnetic properties indicative of dikes from distinct intrusive events. Processing techniques centering fields over sources help the construction of geological maps and allow algebraic expressions to develop automatic interpretation methods. Many of the available applications are based on the properties of the analytical signal amplitude (ASA) (Roest & Pilkington, 1992) or the amplitude of the magnetic anomaly (AMA) (Li et al. 2010; Guo et al. 2014). Both ASA and AMA are not directly measured but instead evaluated from data processing applied to the observed total field anomaly (TFA) by applying conventional linear filtering procedures (Blakely, 1996, chapter 12). AMA and ASA are effective in outlining the distribution of magnetic sources, even in terrains with prevalent remanent magnetization with unknown direction that makes asymmetric the TFA with respect to the dike position. For two-dimensional (2D) sources, ASA (Li, 2006) and AMA (Liu et al., 2015) are invariant with magnetization direction, further simplifying the interpretation of elongated anomalies and magnetic lineaments from dike swarms. Depending on their properties and geometry, such tabular features may have a significant impact on subsurface conditions including the flow regime and exploration for groundwater resources (Cavalcante et al., 2020).

We introduce a discontinuous, interval-defined function obtained from rationing the AMA by its second x-derivative to automatically determine intervals within which a dike unit is expected. The choice for AMA is advised since it is less distorted by shallow sources (geological

noise) and more effective in capturing fields from deeper sources (Li et al., 2010; Liu et al., 2015; Mendonça et al., 2019). The use of AMA second x-derivative aids the identification of intervals where the AMA is concave down to discriminate side-by-side sources with subtle variations in the observed anomalies. For dike swarms, the number of such domains gives a preliminary estimate for a minimum number of prisms that is necessary to explain the observed anomaly, a key parameter for more demanding approaches based on data inversion. The second derivative for AMA was used by Bastani & Pedersen (2001) but, to our knowledge, not applied to individualize adjacent dikes or automatic depth estimates. Since numerical derivation is a noise-enhancing operation, a Tikhonov smoothing approach (Cullum, 1971; Stickel, 2010) was applied to obtain stable derivatives. The smoothening Tikhonov condition effectively works under different noise specifications or variations from applying different gridding methods. A numerical simulation is presented to show the effectiveness of the proposed method in characterizing tightly juxtaposed prisms with variable depth and magnetization properties. A real data application illustrates the automatic approach applied to a dike swarm transect, showing how the approximate results obtained with the proposed automatic procedure does provide a reliable model for geological interpretation as well as a trial solution to input a nonlinear data inversion procedure.

THEORY

The thin sheet model has been used in magnetic data interpretation to represent dikes and geological contacts (Reford, 1964; Hartman et al., 1971) and served as the basis for the well-known Werner deconvolution technique with multiple applications in the interpretation of magnetic data (Ku & Sharp, 1983; Hansen and Simmonds, 1993; Ostrowski et al., 1993). This model is particularly valid to interpret airborne magnetic data acquired at flying heights of about 100 m or more because under such a condition the anomaly from a 10 m to 15 m wide dike, for example, gives a magnetic field equivalent to that one from a sheet. Following Ostrowski et al. (1993), the expressions for the x and z components, $T_x(x)$ and $T_z(x)$, for the magnetic field from a vertical thin sheet, at a profile position (x, z), for $z = 0$ at the ground level, are

$$\begin{cases} T_x(x) = -2Jw\,\dfrac{\cos(i_m)\,z_0 + \sin(i_m)\,(x - x_0)}{(x - x_0)^2 + z_0^2} \\ T_z(x) = 2Jw\,\dfrac{\sin(i_m)\,z_0 - \cos(i_m)\,(x - x_0)}{(x - x_0)^2 + z_0^2} \end{cases}, \qquad (1)$$

where w is the thin sheet thickness, (x_0, z_0) is the coordinate position for the sheet top. For targets with induced magnetization only $J = kT_L$, for k as the rock magnetic susceptibility (dimensionless in the SI), and T_L is the intensity of local main field (nT). The angle i_m, such that $\tan(i_m) = \tan(i)/\cos(\alpha)$, is the magnetization inclination, i, projected at the vertical plane containing the x-axis profile, making a clockwise angle α with respect to the magnetic north. The anomalous vector field, $\mathbf{T}(x) = T_x(x)\mathbf{e}_x + T_z(x)\mathbf{e}_z$, for unitary vectors $\mathbf{e}_x$ and $\mathbf{e}_z$ along the profile and the vertical (positive downward), has field intensity $|\mathbf{T}(x)| \equiv [T_x^2(x) + T_z^2(x)]^{1/2}$ which is equivalent to the AMA as defined by Li et al. (2010). The observed TFA is $T_t(x) = \cos(I_g)\,T_x(x) + \sin(I_g)T_z(x)$, for $\tan(I_g) = \tan(I)/\cos(\alpha - D)$; where I and D are respectively the inclination and declination of the local main field. From the x and z field components in equation 1, the thin sheet AMA is

$$|\mathbf{T}(x)| = \frac{2Jw}{\sqrt{(x-x_0)^2 + z_0^2}} \quad , \quad (2)$$

which is invariant with magnetization inclination i_m. The intensity field in equation 2 also is equivalent to the field from an infinite line of current with intensity $\mathcal{A}_0 = 4\pi w M$, with $M = J/\mu_0$, such as

$$|\mathbf{T}(x)| = \frac{\mu_0}{2\pi} \frac{\mathcal{A}_0}{\sqrt{(x-x_0)^2 + z_0^2}} \quad . \quad (3)$$

To explore the equivalence of the thin sheet response with a line of current, the thin-sheet AMA will be expressed in terms of the equivalent current $\mathcal{A}_0$ instead product $2Jw$. This correspondence reduces the number of model parameters to three unknown variables: $(x_0, z_0, \mathcal{A}_0)$ simplifying model representation. From equation 3, the second x-derivative, $d^2|\mathbf{T}(x)|/dx^2 \equiv |\mathbf{T}(x)|''$, of the intensity field $|\mathbf{T}(x)|$ is

$$|\mathbf{T}(x)|'' = \frac{\mu_0 \mathcal{A}_0}{2\pi} \frac{2(x-x_0)^2 - z_0^2}{[(x-x_0)^2 + z_0^2]^{\frac{5}{2}}} \quad . \quad (4)$$

We introduce the apparent depth function, $z_a(x)$, as the ratio

$$z_a(x) \equiv \sqrt{-\frac{|\mathbf{T}(x)|}{|\mathbf{T}(x)|''}} \quad , \quad (5)$$

as such, defined in the interval where $|\mathbf{T}(x)|'' < 0$, in which the intensity field $|\mathbf{T}(x)|$ is concave down. Based on equations 2 to 5, the z_a depth function for the vertical thin-sheet model is

$$z_a(x) = \frac{(x-x_0)^2 + z_0^2}{\sqrt{z_0^2 - 2(x-x_0)^2}} \quad , \quad (6)$$

defined in the interval $|x - x_0| < z_0/\sqrt{2}$ where the second derivative is negative. For $x = x_0$ the apparent depth-function $z_a(x_0) = z_0$ automatically determines the thin sheet depth as the position of its equivalent line of current. The position x_0 is determined by the minimum of the second derivative $|\mathbf{T}(x)|''$. When plotted for all points with negative second derivative, the $z_a(x)$ function describes a hyperbole-like curve with centred at (x_0, z_0). Once x_0 is determined, the equivalent current $\mathcal{A}_0 \equiv \mathcal{A}_0(x_0)$ can be obtained from equation 4 as

$$\mathcal{A}_0(x_0) = -\frac{2\pi}{\mu_0} z_0^3 \, |\mathbf{T}(x_0)|'' \quad . \quad (7)$$

Figure 1 illustrates a synthetic case in which $z_a(x)$ is evaluated from equation 6 (thus assuming a vertical, infinitely depth-extending thin prism) and numerically from fields evaluated from a

dipping prism with width w. The second derivative of field intensity $|\mathbf{T}(x)|$ for the dipping prism was evaluated numerically by applying a central difference scheme $(T_{i+1} - T_{i-1})/2\delta_x$, with T_{i-1} and T_{i+1} as the evaluated points at positions $x \pm \delta_x$. In Figure 1, $z_a^d(x)$ is the depth function evaluated from data processing applied to the TFA (previously evaluating the corresponding AMA and its second x-derivative), and $z_a^m(x)$ the depth function evaluated from the corresponding thin sheet model according to equation 6. As shown in Figure 1, similar depth functions are obtained from both thick and thin prism models, illustrating that depth estimates with thin sheet models (equation 6) give approximated estimates for wider and dipping prisms. This property of the vertical thin-sheet model was already recognized by Hartman et al. (1971) when developing the Werner deconvolution for automatic aeromagnetic data interpretation. The appropriateness of this approximation will be further illustrated in the section with numerical simulations.

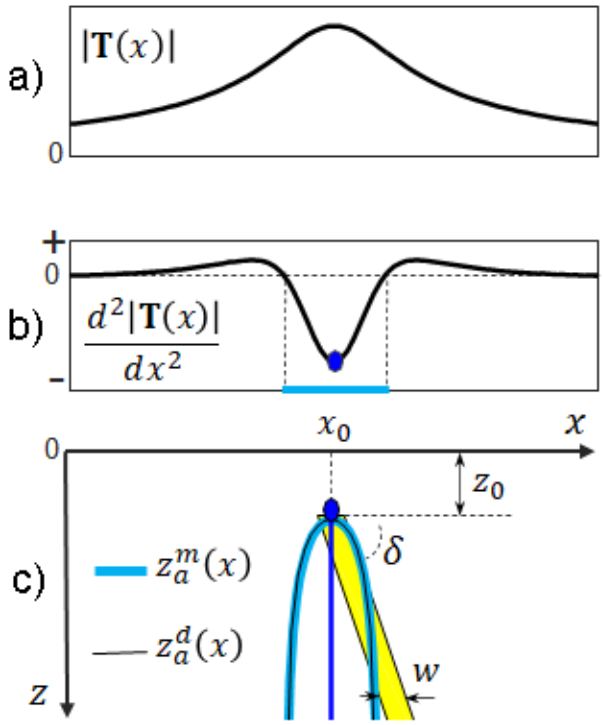

Figure 1 - Schematic representation of field intensity AMA from a dipping-prism model (yellow) and corresponding thin-sheet model (blue): (a) second x-derivative $d^2|\mathbf{T}(x)|/dx^2$; (b) correspondent depth functions evaluated from the thin sheet model, $z_a^m(x)$, (blue line) and from the dipping-prism $z_a^d(x)$ (black line). Points with null second derivative (red circles) and interval (red line) where the depth function $z_a^d(x)$ is defined (negative second derivative). Minimum in the Dipping prim with geometrical (x_0, z_0, w, δ) parameters, the thin sheet with (x_0, z_0) parameters. The AMA field equivalent to a line of current (blue circle) at the top of the thin-sheet. Both prisms with infinite depth extension. Location x_0 is determined by the minimum point in the AMA second x-derivative, depth z_0 determined by $z_a^d(x_0)$.

COMPUTATIONAL IMPLEMENTATION

The evaluation of numerical derivatives configures an unstable operation since amplifying small random variations caused by the noise content in the input data. This kind of instability defines an ill-posed problem that can be solved by applying the Tikhonov regularization theory to stabilize numerical derivatives evaluated from noisy time series or vector data (Eilers, 2003; Stickel, 2010). The regularized derivative procedure was introduced by Cullum (1971) and since then found applications in many fields of the engineering and experimental sciences (Eilers, 2003; Wagner, 2020). The problem can be formulated as a Tikhonov regularization problem (Eilers, 2003; Stickel, 2010). Code implementation was done with the MATLAB function rdiff (Wagner, 2021) with option for Tikhonov regularization (Wagner, 2020; pg. 79). In this implementation the regularization parameter is automatically determined by applying the discrepancy principle criterion. The discrepancy principle (Groetsch, 1984, pg. 43) defines a posteriori strategy based on data input error level. The optimum parameter tunes the residuals Euclidean norm comparable to a scaled factor for the Euclidean norm of the error in data. As in the rdiff implementation, trial regularization parameters are calculated, and that one satisfying the discrepancy criterion then selected. The MATLAB function findpeaks was applied to find the AMA second x-derivative local minima. The findpeaks when applied to a vector v returns the distribution of entries with local maximum satisfying the condition that a local peak in an i-th entry v_i must be larger than its neighboring v_{i-1} and v_{i+1} entries. To find the local minima distribution in v, findpeaks is applied to $-v$.

NUMERICAL SIMULATION

Depth determination with the $z_a(x)$ function is illustrated with program "RunMe_Synthetics.m" implementing up to 10 prismatic models simulating conditions with variable dip and depth, as well as induced and remanent magnetization and variable depth. To each prim in the model is assigned by the auxiliary script "aux01_TestingModels.m" the following parameters: $x_0, z_0, w/2$, δ, M, α, M_{inc}, T_{inc}, z_b, respectively for the x-z top position, half-width, dip angle, magnetization intensity (A/m), dike strike, inclination of magnetization, inclination for the local main field, and depth to the bottom. Figure 2 shows the results corresponding from a particular model (Model 6) as the option 6 in the "aux01_TestingModels.m" script. This model has 6 prisms with tops at different depths (4 km to 9 km, from left to right). TFA and AMA were evaluated along a 100 km long profile at sampling rate Δx=0.35 km. All prisms in this model have induced magnetization ($M_{inc} = T_{inc}$) of 1.0 A/m for T_{inc}=30º and z_b=24 km. AMA response was corrupted with zero-mean, Gaussian noise with a standard deviation of 2 nT to evaluate distortions in evaluating noise enhancing derivatives with simple central difference and Tikhonov regularized schemes. As shown in Figure 2, the z_a function from noisy-data captures the same pattern with noise-free data defining sharped hyperboles with peaks outlining the true depths. The intervals where negative second x-derivative define discontinuous domains where AMA is concave down, the second derivative minima picking the AMA apices with good approximations for prism position x_0.

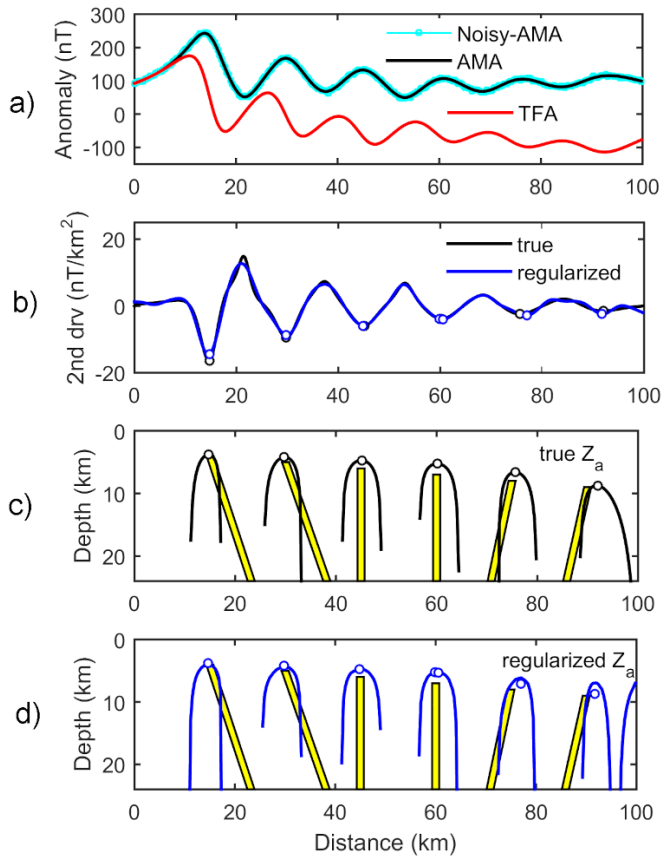

Figure 2 – Numerical simulation with a multi prism model: a) noise-free TFA (red line), noise-free AMA (black) and noise-corrupted AMA (cyan); b) second x-derivative of noise free AMA (black line) and the noise-corrupted AMA (blue line) with regularization and respective local minima (circles); c) true prismatic models (yellow), z_a-function (black hyperboles) from noise-free AMA, $z_a(x_0)$ depth estimates (white circles); d) z_a-function from noise-corrupted AMA (blue). The six prisms in the model have increasing depth to the top, from 4 km depth down to 9 km depth from left-to-right. The dip of the prisms is equal to 70º (1 to 2), 90º (3 to 4) 110º, all prisms with induced magnetization only (local main field with inclination of 30º) and magnetization intensity of 1.0 A/m. Sampling space Δx=0.25 m. This is the model-6 in the "RunMe_Synthetics.m' file. A set of 10 models can be tested with this script.

Figure 3 shows the AMA second x-derivative evaluated from noise-free and noise-corrupted AMA, the Tikhonov regularization providing a stable (non-oscillating) second derivative. The amplitude loss observed in the regularized derivative is caused by the smoothing criterion embedded in the Tikhonov regularization as described in Appendix A. At least for the tested model, this loss in amplitude does not compromise minima location or depth evaluation according to equation 4. Figure 3 illustrates the need for regularization in evaluating the second x-derivative for a noisy data input by comparing the Tikhonov regularized derivative with noise-free and noise corrupted results. Noise in data was simulated by Gaussian, additive, zero-mean pseudo-random values with a standard deviation of 2 nT. The true derivative reference was numerically evaluated by computing fields at points $x_i \pm \delta_x$ with $\delta_x = \Delta x/50$, for data sampling Δx=0.35 m

and applying a central difference scheme. Non-regularized numerical derivative for the noise data applied a central difference scheme directly to the noise-corrupted data. The same corrupted data set was used to evaluate the regularized derivative. As shown in Figure 3, the non-regularized derivative amplifies the noise content leading to meaningless results. The regularized approach, otherwise, provides reliable results reproducing the noise-free derivative curve despite a minor amplitude loss caused by the smoothing criterion the Tikhonov regularization applies.

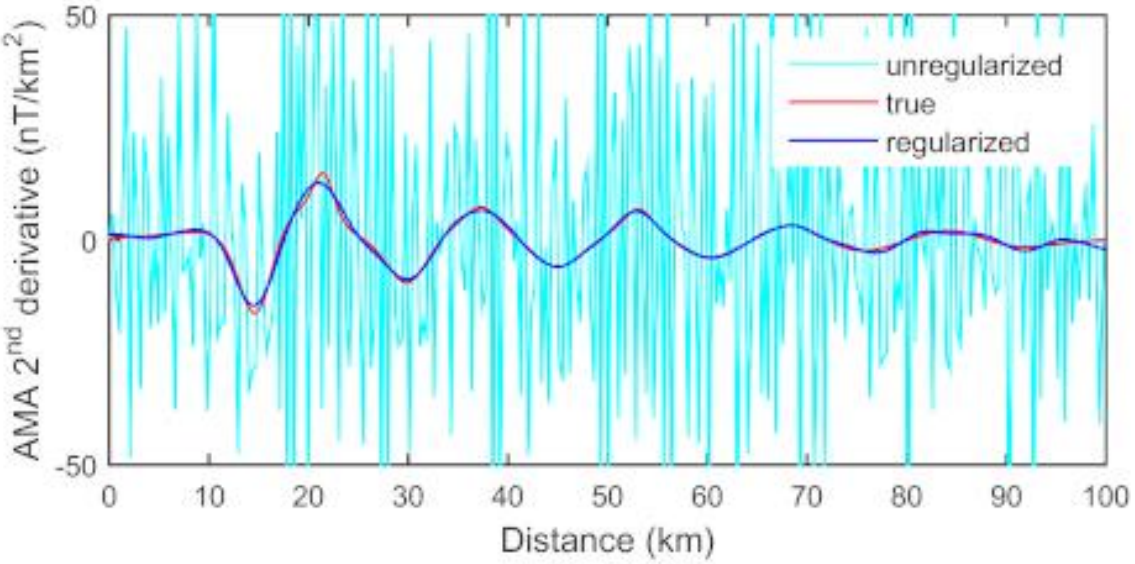

Figure 3 –AMA profile second numerical derivatives: a) noise-free (red line) and noise-corrupted (cyan) AMA profile, and regularized 2nd derivative (blue). Pseudo random noise in data generated assuming a zero-mean Gaussian distribution with standard deviation of 2 nT. True derivative numerically evaluated with a central difference scheme at points $x_i \pm \delta_x$ with $\delta_x = \Delta x/50$. AMA profile from model in Figure 2.

Table 1 with true and estimated model parameters shows that location and depth errors (expressed in terms of the sampling space Δx=0.35 km) are below $3\Delta x$. Error scaling by the sampling spacing establishes a fair ground to compare deeper and shallower sources or situated away from the origin. For an automatic technique, this margin of error can be regarded as satisfactory considering the noise level in data and the simple approximation of wider dipping prisms with a vertical thin sheet model. Worth to note is that model parameters were determined without any data inversion approach, but simply by evaluating the ratio between two data processing products (the AMA and its second derivative). The amplitude factor A_0 have a higher error margin (in %) by taking as reference the product $4\pi Mw$ for each dike. Low accuracy in A_0 may prevent the identification of same size dikes with contrasting magnetization intensity but still valuable as semi-quantitative discrimination of dike populations as well as dike locations.

	True model			z_a-estimates			Errors		
	x_0 (m)	z_0 (m)	$4\pi Mw$ (A)	x_0 (m)	z_0 (m)	$\mathcal{A}_0$ (A)	x_0 ($\times \Delta x$)	z_0 ($\times \Delta x$)	$\mathcal{A}_0$ (%)
1	8	4	7.5	6.8	4.5	13.7	4.8	2.0	83
2	15	3	7.5	14.6	2.9	9.1	1.6	0.4	21
3	22	4	7.5	21.5	3.1	5.7	2.0	3.6	24
4	29	3	7.5	28.8	2.6	6.8	0.8	1.6	9
5	36	4	7.5	35.7	2.9	5.0	1.2	4.4	33
6	43	3	7.5	42.9	2.9	8.5	0.4	0.4	13
7	50	6	11.3	50.9	5.0	8.2	3.6	4.0	27
8	60	6	11.3	60.3	4.4	6.8	1.2	6.4	40
9	70	6	11.3	70.4	4.9	9.1	1.6	4.4	19
10	80	6	11.3	80.7	5.6	12.3	2.8	1.6	9
11	90	6	11.3	91.4	6.2	16.7	5.6	0.8	48

Table 1 – Model parameters for thick (yellow prism) and thin sheet (black) prismatic models and correspondence of z_a-function from both models, z_a^m from the thin-sheet model and z_a^d from observed data from a true wide prism. Both prisms with top at x_0 and z_0, the wider prism with dipping angle δ and width w. Magnetization-to-width product $4\pi Mw$ for a thick prism and correspondent amplitude term A_0 evaluated with the thin sheet model. Errors evaluated with respect to the true model value. Sampling space $\Delta x = 1.5$ m.

REAL DATA APPLICATION

The proposed technique is applied to a magnetic profile across the southern branch of the northwest portion of Ponta Grossa Dike Swarm (PGDS), at the eastern border of the Phanerozoic Paraná Basin, in the Paraná State, Brazil (Figure 4a). The background geology (Figure 4c) is composed by Tonian to Ediacaran metavolcano-sedimentary sequences and arc-related granite stocks (Passarelli et al., 2019). The Precambrian basement is part of the Apiaí Terrane, a tectonic block of the Neoproterozoic Ribeira Belt recording the last stages of the West Gondwana amalgamation (Campanha et al., 2019). The northern portion of the area is covered by Devonian sandstones of the Furnas Formation. Only few diabase dikes of the Cretaceous Serra Geral Formation (Renne et al., 1996) are mapped from ground-based geology. The available magnetic data was acquired with 500 m spaced, North-South flight lines at constant 100 m height above the ground. The xyz-database is made available by the CPRM- Brazilian Geological Survey (https://geosgb.cprm.gov.br/) under identification of survey 1095, Paraná-Santa Catarina database. The evaluation of AMA from gridded TFA data required the evaluation of the x, y, and z components of the anomalous magnetic field by applying conventional phase transformation filtering (Blakely, 1996, pg. 328), as implemented in the component changing options of the GEOSOFT-Oasis Montaj version 9.10. This CPRM survey was developed in 2011, for a local main field with intensity of 22640 nT, inclination of -34º, and declination of -18º. The entire data set was processed at a regular grid of 50 m and resampled at the same rate along profile PP' transverse to the dikes. The extension and shape of the observed magnetic lineaments suggest the existence of multiple non-outcropping dikes, coincident with the mean strike (N30W) of the

outcropping dikes. As in other cases, the extension and distribution of dike swarms in the Brazilian shield have been inferred from their aeromagnetic expressions (Pessano et al., 2021), not directly from outcropping inspections.

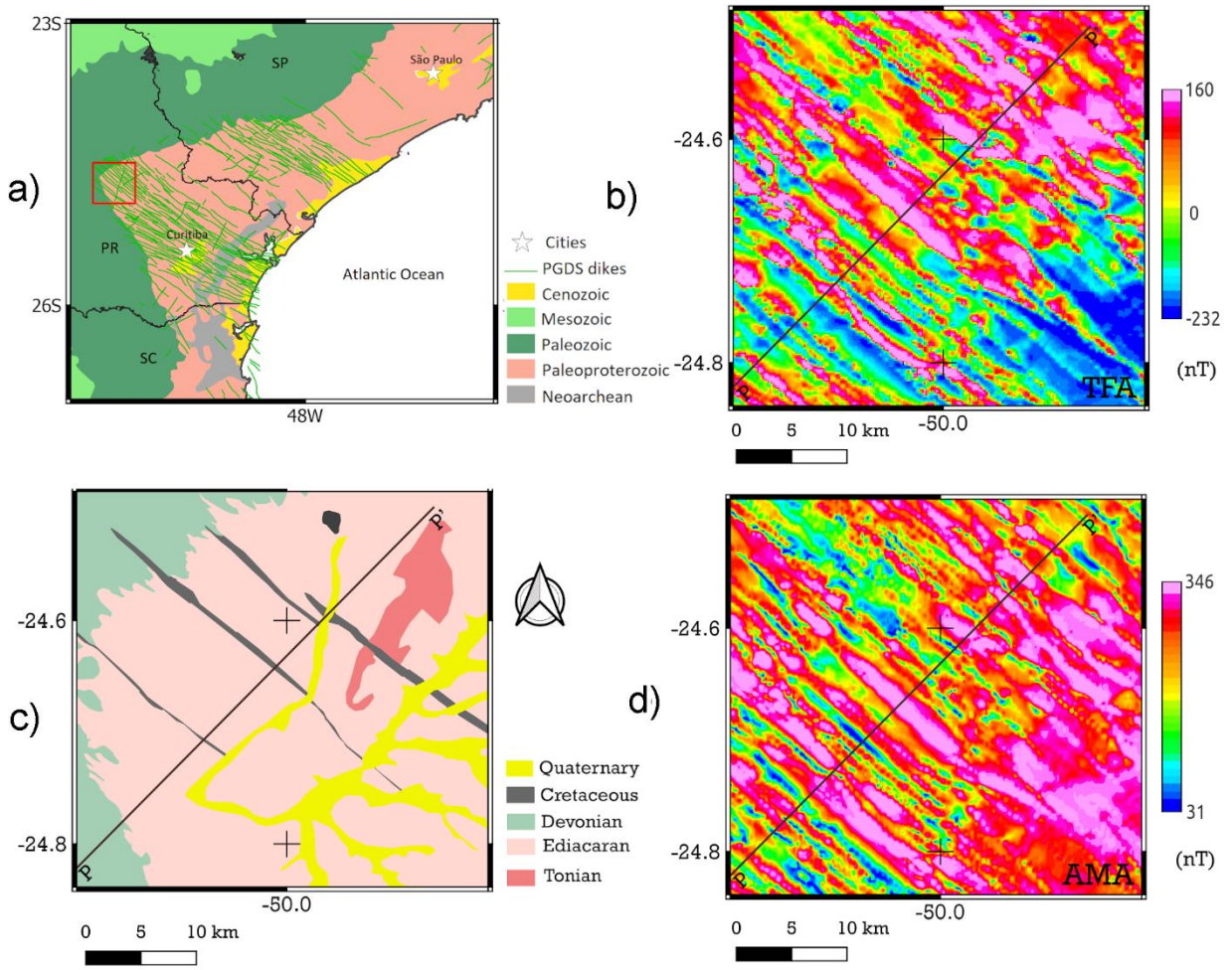

Figure 4 – Ponta Grossa Dike Swarm (PGDS) localization and magnetic anomalies from multiple dikes: a) PGDS localization at the Precambrian Brazilian Shield (Neoarchean to Proterozoic), the study area (red polygon) at the northern portion of the southern branch of the swarm; c) schematic geological map for the study area with Tonian and Ediacaran Precambrian blocks and outcropping Cretaceous dikes; b) Total field anomaly (TFA) and d) Amplitude magnetic anomaly (AMA). The extension of the elongated magnetic anomalies in TFA; and AMA suggests the existence of non-outcropping dikes closely allocated side-by-side. Profile PP' investigated with z_a-depth function and non-linear data inversion.

The magnetic anomaly along profile P-P' in Figure 4 was inverted by Cavalcante et al. (2020), according to an inversion approach defining a trial number of dikes as given by the well-shaped peaks in the AMA profile. A preliminary model fitting the AMA profile was used to fit the TFA profile, at this stage by interactively including additional prisms to improve data fitting at specific portions of the profile. As shown in Figure 5, this approach produced a model with 51

thin-sheets, by minimizing a non-linear misfit function with 204 unknown parameters. As implemented by Cavalcante et al. (2020), each thin sheet in the model has four unknown parameters (x_0, z_0, A_0, i_m), parameter A_0 such that $3.39 \leq A_0 \leq 1695$ A/m, the lower bound corresponding to the product between the minimum dike width (0.3 m) by the minimum magnetization intensity (0.68 A/m); the upper bound given by the product of maximum width (500 m) and maximum magnetization intensity (3.39 A/m). Lower and upper bounds for dike width and magnetization were provided by Raposo (1995). Model parameters and corresponding TFA data fitting from Cavalcante et al. (2020) are presented in Figure 5, the magnetization direction represented as "normal" (aligned to the present main field) and "reverse". The existence of reverse magnetization has been recognized in paleomagnetic studies (Raposo, 1995) and inferred by the change in the negative-to-positive pattern (from South-to-North) as expected from TFA anomalies with induced magnetization only.

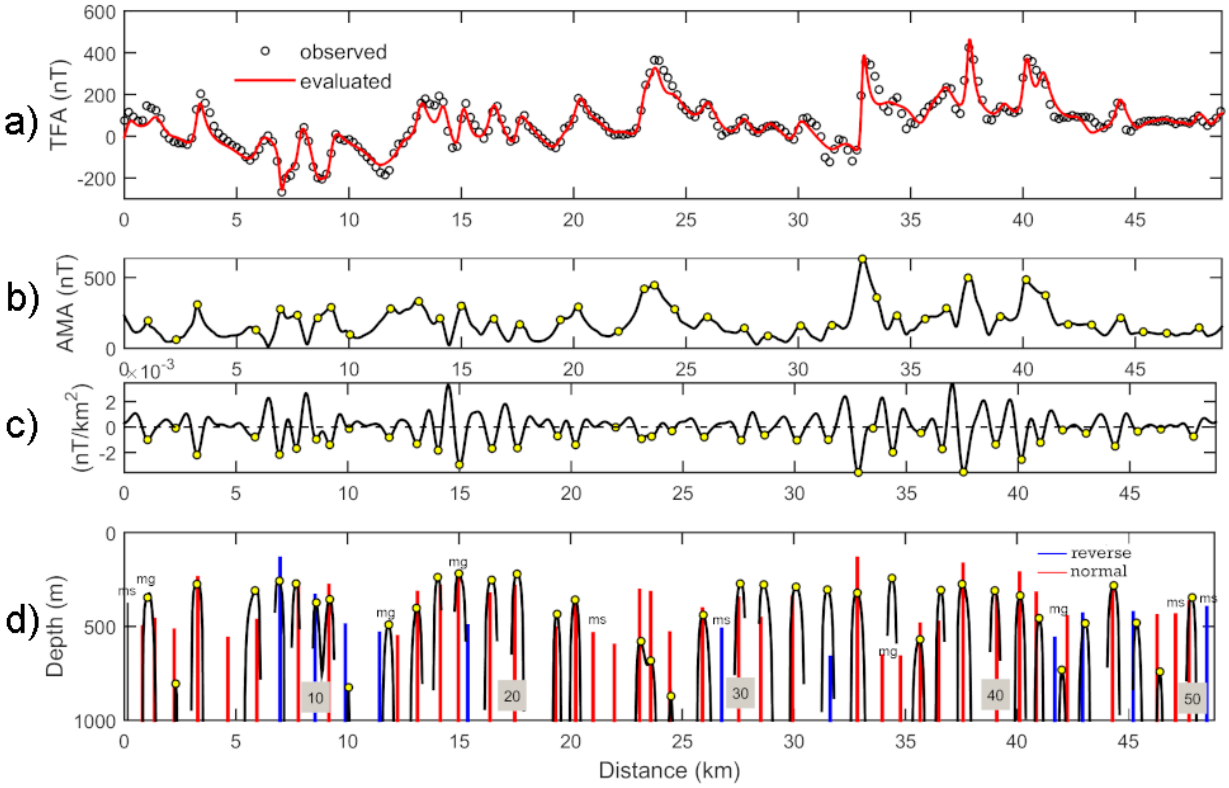

Figure 5 – Profile PP' across the southern branch of the PGDS: a) observed TFA (square) and model evaluated fitting data with 51 thin sheets as obtained by Cavalcante et al. (2020); b) AMA obtained from processing the TFA profile and points with local maximum (circles); c) Tikhonov regularized second x-derivative and points with local minima (circles); d) thin sheet model with normal (red) and reverse (blue) magnetization as in Cavalcante et al. (2020) and corresponding $z_a(x)$ depth function (black line) and maximum points $z_a(x_0)$ for local minima x_0 in the second derivative profile. Missed (ms) dikes recognized in the non-linear inversion but not as minima points in the second derivative. Merged (mg) dikes identified as two bodies in the non-linear inversion but just as a single one by second-derivative minima. Prism numbers 10, 20, 30, 40, and 50 to facilitate the comparison of automatic and data inversion parameters as in Table 2.

Table 2 shows model parameters from data inversion and the corresponding ones from the automatic depth function. As in Table 2 and Figure 5, there is a good agreement between both models. Most of the dikes in the inverted model are situated close to AMA peaks (Figure 5b) and were automatically recognized by the local minima of the AMA regularized second derivative (Figure 6c). A set of local minima occurs at the AMA flanks, in places where AMA curvature show inflections or asymmetrical decay with respect to the local main peak. From the 51 thin sheets in the inverted model, 36 were automatically identified, 23 of them with x_0 error less than $2\Delta x$, 18 of them with z_0 error less than $2\Delta x$. A set of 10 prisms at places with no sharp AMA apex is marked as "merged', a condition in which two prisms in the inverted model are mapped as a single prism by the depth function. The automatic estimate for the merged prisms 18 and 19, for example, recovers the location and depth for the prism 18 meanwhile missing the adjacent deeper prism. Only five prisms in the inverted model were not identified by the depth function as marked as missed in Figure 5 and Table 2. Local minima oscillations near the zero in the second derivative profile assign deep-seated dikes, which for the sake of graphical representation were clipped to a depth of 1000 m (Figure 5d). As in the numerical simulation, the errors in current intensity $\mathcal{A}_0$ are high but still useful as a trial model for a nonlinear data inversion procedure. Location and depth parameters, otherwise, are accurate enough to be useful in semiquantitative or geological interpretation. The inclusion of additional dikes undetected by the automatic procedure is justified when additional constraints on depth or magnetization properties are incorporated. This criterion justifies the inclusion of prisms without sharped expressions in the observed fields, but necessary to keep consistency with geological and petrophysical constraints. The good agreement between the inverted and automatically estimated model parameter justifies the use of the automatic solution in preliminary interpretation stages as well as to obtain a trial model to input more complex data inversion routines.

CONCLUSIONS

The automatic parameter estimator by using the ratio of the AMA by its second x-derivative shows efficiency in identifying closed juxtaposed dikes as observed in continental dike swarms. The obtained results at a transect of the PGDS are in good agreement with those ones obtained with data inversion. The automatic model representation provided by the z_a function can be used as an objective criterion to establish a minor number of dikes necessary to explain the observed data set as well as provide reliable estimates for dike location, the depth to the top, and amplitude factor expressing the magnetization to prism-width product for a thin prism or the current intensity for an equivalent line of current. We propose that solutions automatically obtained with the z_a-function should be used as trial solutions for more demanding data inversion approaches. In doing so, existing airborne magnetic data sets may be rapidly explored using the presented automated approach to highlight priority areas for subsequent model refinement or further detailed analysis. Location and depth obtained with the automatic procedure accurately recover the model parameters obtained from nonlinear data inversion suggesting the utility of the proposed procedure in providing preliminary model inference from complex anomalies generated by multiphase dike swarms.

	Inverted			z_a-function			Error		
	x_0 (km)	z_0 (m)	$\mathcal{A}_0$ (A)	x_0 (km)	z_0 (m)	$\mathcal{A}_0$ (A)	x_0 ($\times \Delta x$)	z_0 ($\times \Delta x$)	$\mathcal{A}_0$ (%)
1	0.1	378	340	missed					
2	0.8	502	119	merged					
3	1.4	464	340	merged					
4	2.2	520	121	2.30	806	396	1.4	5.7	226
5	3.3	241	289	3.30	265	399	0.2	0.5	38
6	4.6	564	41	4.80	1000	< 1	3.1	8.7	-
7	5.9	468	331	5.90	303	211	0.8	3.3	36
8	7.0	138	140	6.90	247	312	1.6	2.2	123
9	7.8	285	339	7.70	273	341	1.9	0.2	1
10	8.6	335	229	8.60	373	495	1.0	0.8	116
11	9.2	282	305	9.20	357	631	0.6	1.5	107
12	9.9	492	46	10.05	824	635	3.0	6.6	1291
13	11.4	536	174	merged					
14	12.2	555	331	merged					
15	13.1	319	340	13.15	398	826	0.3	1.6	143
16	14.2	288	275	14.05	238	249	2.1	1.0	9
17	15.0	248	336	15.00	218	307	0.7	0.6	9
18	15.4	498	216	merged					
19	16.4	328	339	merged					
20	17.5	287	249	17.60	221	177	2.1	1.3	29
21	19.3	509	271	19.35	433	527	0.7	1.5	95
22	20.2	354	328	20.20	358	641	0.5	0.1	95
23	21.0	539	124	missed					
24	22.0	601	164	22.10	1000	< 1	2.8	8.0	-
25	23.1	309	340	23.10	577	1714	0.3	5.4	404
26	23.6	320	340	23.60	681	2308	0.3	7.2	578
27	24.4	534	292	24.50	871	1935	1.1	6.7	563
28	25.9	406	269	25.90	437	640	0.1	0.6	138
29	26.8	515	55	missed					
30	27.5	350	180	27.65	270	192	2.4	1.6	7
31	28.5	458	230	28.65	277	1651	2.6	3.6	43
32	29.9	344	218	30.10	289	253	3.3	1.1	16
33	31.6	665	340	31.50	304	282	2.7	7.2	17
34	32.8	137	340	32.85	320	1177	0.0	3.7	246
35	34.0	657	340	merged					
36	34.8	663	291	merged					
37	35.7	488	340	35.65	570	863	0.3	1.6	153
38	36.5	478	340	36.60	307	498	2.1	3.4	46
39	37.6	169	340	37.55	275	735	0.8	2.1	116
40	39.1	344	158	39.00	309	399	1.9	0.7	153
41	40.1	216	340	40.15	336	969	0.6	2.4	185
42	40.9	323	340	41.00	457	1155	2.7	2.7	73
43	41.7	563	426	41.25	1000	< 1	9.0	8.7	-
44	42.3	448	931	merged					
45	42.9	435	2045	merged					
46	44.3	301	3050	44.30	280	321	0.3	0.4	32
47	45.2	427	1665	45.35	481	388	2.7	1.1	193
48	46.3	444	835	46.40	741	610	2.4	6.0	818
49	47.1	439	964	missed					
50	47.7	371	2446	47.80	345	298	1.6	0.5	53
51	48.5	400	2361	missed					

Table 2- Thin sheet model parameters with 51 thin sheets obtained from non-linear data inversion (Cavalcante et al., 2020) and corresponding values obtained with the automatic z_a depth function. Errors in x_0 and z_0 evaluated as multiple of the grid space Δx= 50 m. Errors in A_0 evaluated as a percent of the value obtained with data inversion. Prism numbering from 1 to 51 as marked for multiples of 10 in profile PP' of Figure 5.

ACKNOWLEDGMENTS

Thanks to Jakub Wagner for developments with regularized derivatives. This study was supported by FAPESP 2019/20172-7; CNPq 304450/2022-7 and in part by the Coordenação de Aperfeiçoamento de Pessoal de Nível Superior - Brasil (CAPES) - Finance Code 001

REFERENCES

Aster, R.C., B. Borchers, & C. Thurber, 2012, Parameter estimation and inverse problems, 2nd Edition. Academic Press.

Blakely, R.J., 1996, Potential theory in gravity and magnetic applications. Cambridge University Press.

Bastani, M., & L.B. Pedersen, 2001, Automatic interpretation of magnetic dike parameters using the analytical signal technique: Geophysics, (66)551-561. DOI:10.1190/1.1444946.

Campanha, G. A., F.M. Faleiros, P.A. Cawood, D.I. Cabrita, B.V. Ribeiro, & M.A. Basei, 2019, The Tonian Embu Complex in the Ribeira Belt (Brazil): revision, depositional, age and setting

in Rodinia and West Gondwana: Precambrian Research, (320)31-34. DOI:10.1016/j.precamres.2018.10.010.

Cavalcante, F.L., C.A. Mendonça, S.U. Ofterdinger, & O.A. de Souza-Filho, 2020, Well productivity in the Ponta Grossa dike Swarm, Brazil: An integrated study with magnetic data inversion and clustering analysis of model solutions: Journal of Hydrology, 588. 125079. DOI:10.1016/j.jhydrol.2020.125079.

Cullum, J., 1971, Numerical differentiation and regularization: SIAM J. Numer. Anal., 8(2), 254-265. DOI:10.1137/0708026.

Eilers, P., 2003, A perfect smother: Analytical Chemistry, 75(14), 3631–3636. DOI: 10.1021/ac034173t.

Groetsch, C., 1984, The theory of Tikhonov regularization for Fredholm equations of the first kind. Pitman Publishing.

Guo, L., X. Meng, & G. Zhang, 2014, Three-dimensional correlation imaging for total amplitude magnetic anomaly and normalized source strength in the presence of strong remanent magnetization: Journal of Applied Geophysics, 11, 121-128. DOI:10.1016/j.jappgeo.2014.10.007.

Hansen, R.O., & M. Simmonds, 1993, Multiple-source Werner deconvolution: Geophysics, 58(12), 1792-1800. DOI:10.1190/1.1443394.

Hartman, R.R., D.J. Teskey, & J.L. Friedberg, 1971, A system for rapid digital aeromagnetic interpretation: Geophysics, 36(5), 891-918. DOI:10.1190/1.1440223.

Ku, C.C., & J.A. Sharp, 1983, Werner deconvolution for automated magnetic interpretation and its refinement using Marquardt's inverse modeling: Geophysics, 48(6), 754-774. DOI:10.1190/1.1441505.

Li, X., 2006, Understanding 3D analytic signal amplitude: Geophysics, 71(2), L13-L16. DOI:10.1190/1.2184367.

Li, Y., S.E. Shearer, M.M. Haney, & N. Dannemiller, 2010, Comprehensive approaches to 3D inversion of magnetic data affected by remanent magnetization: Geophysics, 75(1), L1-L11. DOI:10.1190/1.3294766.

Liu, S., X. Hu, Y. Xi, T. Liu, & S. Xu, 2015, 2D sequential inversion of total magnitude and total magnetic anomaly data affected by remanent magnetization: Geophysics, 80(3), K1-K12. DOI:10.1190/geo2014-0019.1.

Mendonça, C.A., W.P. Soares, & F.L. Cavalcante, 2019, Annihilator transform for magnetic lineaments removal in dike swarms: Geophysics, 84(4), J31-J41. DOI:10.1190/geo2018-0308.1.

Ostrowski, J.S., M. Pilkington, & D.J. Teskey, 1993, Werner deconvolution for variable altitude aeromagnetic data: Geophysics, 58(10), 1481-1490. DOI:10.1190/1.1443362Passarelli, C. R., S.K. Verma, I. McReath, M.A. Basei, & O. Siga-Jr, 2019, Tracing the history from Rodinia break-up to Gondwana amalgamation in the Embu Terrane, southern Ribeira Belt, Brazil: Lithos, (342-343), 1-17. DOI:10.1016/j.lithos.2019.05.024.

Pessano, P.C., C.E. Ganade, M. Tupinambá, & W. Teixeira, 2021, Updated map of the mafic dike swarms of Brazil based on airborne geophysical data: Journal of South American Earth Sciences: (107), 103076. DOI: 10.1016/j.jsames.2020.103076.

Raposo, M., 1995, Episódios intrusivos no Arco de Ponta Grossa determinados através de um estudo paleomagnéticos: Revista Brasileira de Geociências, (25)3-19. DOI:10.25249/0375-7536.1995319.

Reford, M.S., 1964, Magnetic anomalies over thin sheets: Geophysics, 29(4), 532-536. DOI:10.1190/1.1439388.

Renne, P.R., K. Deckart, M. Ernesto, G. Féraud, & E.M. Piccirillo, 1996, Age of the Ponta Grossa dike swarm (Brazil), and implications to Paraná flood volcanism: Earth and Planetary Science Letters, 144, 199-211. DOI:10.1016/0012-821X(96)00155-0.

Roest, W.R., J. Verhoef, & M. Pilkington, 1992, Magnetic interpretation using the 3-D analytic signal: Geophysics, 57(1), 116-125. DOI:10.1190/1.1443174.

Stickel, J., 2010, Data smoothing and numerical differentiation by a regularization method: Computers & Chemical Engineering, 34(4), 467-475. DOI: 10.1016/j.compchemeng.2009.10.007.

Wagner, J., 2020, Regularized differentiation of measurement data in systems for healthcare-oriented monitoring of elderly persons. PhD Thesis, Warsaw University of Technology: https://repo.pw.edu.pl/docstore/download/WUT11e668e05d284ea4b708c21ca9ca4803/ [July 16, 2021].

Wagner, J., 2021, Regularized numerical differentiation. Accessed on July 17. https://www.mathworks.com/matlabcentral/fileexchange/74165